Pervaporation and Vacuum Membrane Distillation Processes: Modeling and Experiments

Mohamed Khayet
Dept. of Applied Physics I, Faculty of Physics, University Complutense of Madrid, Madrid, Spain

Takeshi Matsuura
Industrial Membrane Research Institute, Dept. of Chemical Engineering, University of Ottawa, Ottawa, Ontario K1N 6N5, Canada

DOI 10.1002/aic.10161
Published online in Wiley InterScience (www.interscience.wiley.com).

Two separation processes, pervaporation (PV) and vacuum membrane distillation (VMD), were studied using polyvinylidene fluoride (PVDF) flat-sheet membranes for the separation of chloroform–water mixtures. Both PV and VMD membranes were prepared using the phase-inversion method and the same polymer material. VMD membranes with different pore sizes were prepared using pure water as a pore-forming additive in the PVDF/dimethylacetamide casting solution, whereas PV membranes were obtained with higher polymer concentration, without nonsolvent additives and with solvent evaporation before gelation. The mean pore size, porosity, and pore size distributions of the VMD membranes were determined. Water and formamide advancing and receding contact angles of PV membranes were measured. The swelling degree, the solubility parameter of PV membranes, and the interaction of the permeants with the PVDF polymer were calculated. In the VMD process, a more general theoretical model that considers the pore size distribution, the solution–diffusion contribution through nonporous membrane portion, and the gas transport mechanisms through membrane pores was developed based on the kinetic theory of gases. The contribution of each mechanism was analyzed. A comparative study was made between both membrane separation technologies. © 2004 American Institute of Chemical Engineers *AIChE J,* 50: 1697–1712, 2004
Keywords: vacuum membrane distillation, pervaporation, heat and mass transfer, volatile organic compound, separation

Introduction

Pervaporation (PV) and vacuum membrane distillation (VMD) are membrane separation processes in which the upstream side of the membrane is in contact with feed liquid while vacuum is applied on the downstream side of the membrane. Both techniques are similar and often confused. The fundamental difference between them, as can be observed in Figure 1, is the role that the membrane plays in the separation. VMD uses porous and hydrophobic membranes that act only as support for the vapor–liquid interface and do not contribute in the separation performance. On the contrary, pervaporation requires dense and selective membranes and the separation is based on the relative solubility and diffusivity of each component in the membrane material.

In VMD, because of the hydrophobic nature of the membranes, the feed cannot penetrate inside dried membrane pores unless a transmembrane hydrostatic pressure exceeds the "liquid entry pressure of water (*LEPw*)," which is characteristic of each membrane (Smolder and Franken, 1989). This condition

Correspondence concerning this article should be addressed to M. Khayet at khayetm@fis.ucm.es.

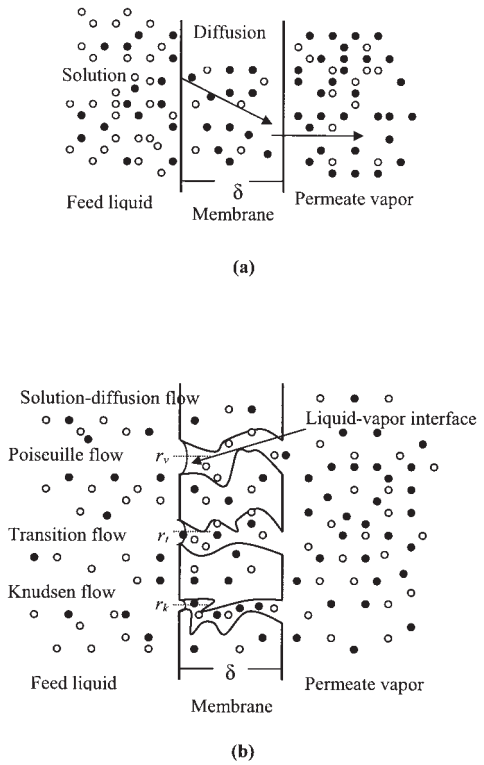

Figure 1. Mechanisms of mass transfer in PV (a) and VMD (b).

results in the formation of a liquid–vapor interface at the entrance of each membrane pore. Therefore, because a vapor pressure difference—which is the driving force in VMD—is maintained between both sides of the membrane pores, molecules evaporate from the feed side of the membrane, cross the pores in the vapor phase, and condense outside the membrane module by means of nitrogen-filled cold traps. In pervaporation, the mass transport is generally described by a solution–diffusion mechanism. The model consists of solution of the liquid feed penetrant molecules at the upstream side, diffusion through the membrane, and desorption into the vapor phase at the downstream side of the membrane. Thus, the PV selectivity and permeation are governed by solubility and diffusivity of each component of the feed mixture to be separated. In this process, the permeant vaporizes somewhere between the upstream and the downstream side of the membrane; therefore, the permeate is obtained as vapor and also collected by nitrogen-filled cold traps.

As a consequence, VMD typically achieves fluxes that are several orders of magnitude higher than pervaporation fluxes and the selectivity in pervaporation is considerably higher than that in VMD. This phenomenon is attributed to the fact that in VMD the selectivity is mainly determined by the vapor–liquid equilibrium conditions at the membrane–solution interface, although the diffusion across the porous membrane may impart some favor to the flux of lighter molecules.

As a separation tool, pervaporation is often used for the separation of organic/organic mixtures and organic/water mixtures; however, VMD is most often used for the removal of volatile organic compounds from dilute aqueous solutions because of the risk of pore wetting (Peña et al., 1997). In fact the possibility of membrane wetting in VMD is higher than that in the other membrane distillation (MD) configurations (Lawson and Lloyd, 1997; Mengual and Peña, 1997), that is, direct contact membrane distillation (DCMD), sweeping gas membrane distillation (SGMD), and air gap membrane distillation (AGMD).

On the other hand, depending on the permeating component, two main areas of PV can be identified: (1) hydrophilic PV and (2) organophilic PV (that is, hydrophobic PV in aqueous–organic mixtures). In the first case, the target compound—water—is separated from an aqueous–organic mixture by being preferentially permeated through the membrane, whereas in the second case the target organic compounds are separated from an aqueous–organic mixture or from an organic–organic mixture by being preferentially permeated through the membrane.

Recently, a study of parallelism and differences of PV and VMD techniques in the removal of volatile organic compounds (VOCs), such as chloroform, from aqueous streams was made by Urtiaga et al. (1999, 2000, 2001). The comparison was performed on the basis of the simulation of the chloroform separation with time using commercial polydimethylsiloxane (PDMS) hollow fibers for PV experiments and microporous polypropylene (PP) hollow fibers for VMD experiments. However, different fluid dynamic conditions, which may affect both concentration and temperature polarization in the feed side as well as different downstream pressures, were used. Nevertheless, among other operating, parameters the selectivity of the VMD process was influenced by the downstream pressure (Bandini et al., 1997). It was found that the rate of chloroform removal was the same in both PV and VMD systems because the kinetics of the chloroform removal are limited by the transport of chloroform in the aqueous phase and increasing Reynolds number conferred a slight advantage to the PV system. In fact, when comparing PV and VMD processes the same membrane material, identical geometrical characteristics of the system, and the same operating conditions must be used.

Compared to the number of reported studies on PV membranes, very few works have been carried out on the design of membranes for MD (Lawson and Lloyd, 1997). Generally, MD is conducted using microporous and hydrophobic membranes prepared especially for microfiltration purposes. Those membranes are typically fabricated from polytetrafluoroethylene (PTFE), polypropylene (PP), or polyvinylidene fluoride (PVDF) materials. Their pore sizes range from 100 Å (0.01 μm) to 1 μm. A good porous MD membrane should exhibit high permeability or low membrane resistance, high *LEPw*, low thermal conductivity, good thermal stability, and excellent chemical resistance to feed streams. The preparation and characterization of MD membranes were the aim of our previous study (Khayet and Matsuura, 2001). PVDF membranes with different pore sizes and porosities were successfully prepared. Those membranes were characterized in terms of their nonwettability, pore size, and porosity measurements using bubble-point and gas permeation tests. In the present work, pervaporation membranes with different thicknesses were prepared from the same polymer. The separation experiments were carried out by use of the same system for both VMD and PV, under similar operating conditions, using both pure water and chloroform/water binary mixtures as feed.

Within the last decade, several similar mathematical models

in MD have been presented (Bandini et al., 1997; Khayet et al., 2000, 2001; Lawson and Lloyd, 1996, 1997). The analyses were based on the assumption that gas permeates through a porous membrane constituting three contributions: Knudsen flow, Poisseuille flow, and molecular diffusion flow and the transition between them. The dusty gas model is frequently used to calculate the MD fluxes and the molecular diffusion flow is not considered in VMD configuration (Bandini et al., 1997; Lawson and Lloyd, 1996, 1997). However the solution–diffusion flow through the nonporous portion of the membrane is not considered in spite of the existence of a high "affinity" (that is, close solubility parameters) between the species to be separated and the membrane material. Moreover, the pore size is important for elucidating the physical nature of the mass transport through the membrane. Most of the literature reports have used the average pore size to calculate the mass fluxes. Nevertheless, because of pore size distribution of the membranes, more than one mechanism of mass transport can simultaneously occur.

Recently, the effect of pore size distribution on mass transport in DCMD was studied assuming Gaussian (symmetric) and logarithmic (asymmetric) distributions (Laganà et al., 2000). It was found that the flux calculated assuming that all pores have the same diameter and the flux calculated with symmetric (Gaussian) function are very similar; whereas the mass flux calculated using an asymmetric distribution was higher than the flux calculated using a symmetric function and both predicted fluxes were lower than the experimental value. Moreover, Martínez et al. (2002) obtained pore size distributions of three hydrophobic porous membranes from air–liquid displacement measurements and the transmembrane water vapor permeabilities in DCMD process were calculated. The agreement with the experimental results was considered good. Phattaranawik et al. (2002) stated that the influence of pore size distribution (that is, the log-normal distribution) on water fluxes in DCMD was insignificant because of the large membrane pore size used (0.2–0.45 μm) and reported that the mass transfer model with the assumptions of single pore size is adequate to describe mass transport in DCMD. However, in their calculation an adjustment factor (that is, tortuosity factor of 2) was assumed for all membranes.

One of the purposes of this article is to provide a more general approach to determine mass transport in VMD distillation, taking into account the solution–diffusion through the nonporous membrane part; the Knudsen flow, transition flow, and Poisseuille flow through the membrane pores; and the pore size distribution of the MD membranes determined by the dry/wet flow method. The major difference between the current work and the previous works is that the previous works mathematically treated the porosity and pore size the same for Knudsen, transition, and Poissueille regions and no distinction was made between the porosity in each region.

Experimental

Materials

The polymer used in this work is polyvinylidene fluoride (PVDF; Kynar® grade 740, Elf Autochem, Philadelphia, PA). *N*,*N*-Dimethylacetamide (DMAC; synthesis grade, >99%, Merck, Darmstadt, Germany) was used as solvent to prepare the polymer casting solution. Pure water was used as a nonsolvent additive for pore making. Ethanol (GR grade, 99%, Merck) was used for the solvent-exchange method. Distilled water and formamide (99%, BDH Chemicals, Toronto, Canada) were used for the contact angle measurement and chloroform (99.8%, Aldrich Chemical, Milwaukee, WI) was used to conduct the PV and VMD experiments.

Membrane preparation

Pervaporation and vacuum membrane distillation flat-sheet membranes were prepared by the phase-inversion method.

To prepare pervaporation membranes, PVDF was dissolved in DMAC (PVDF 20 wt. %) and stirred at about 328 K for about 12 h to ensure the complete dissolution of the polymer. The polymer dope prepared was transparent and homogeneous at room temperature. The resulted solutions were filtered through a 0.5-μm Teflon filter, under a pressure of 2.41×10^5 Pa, to remove nonsoluble contaminants. The mixture was then degassed overnight at room temperature. The polymer solution was poured onto glass plates for casting at room temperature using casting bars to allow preparation of membranes with different thicknesses. The cast films together with the glass plates were placed in an oven with forced-air circulation for solvent (DMAC) evaporation under controlled temperature of about 373 K for 300 s. The films were further immersed in distilled water at about 294 K for at least 1 h. During gelation, the membrane spontaneously peeled off from the glass plate. Those membranes were subjected to solvent exchange after gelation. First, the membranes were immersed for about 4 h in an aqueous ethanol solution (50 wt. %) and then in pure ethanol for 24 h. Furthermore, the membranes were dried at room temperature for about 6 h and then dried under vacuum for 24 h.

For the preparation of the VMD membranes, water was used as a nonsolvent additive for pore making. PVDF (15 wt. %) was added to the water/DMAC mixtures, in which water content was varied from 0 to 5.1 wt. %. More details concerning MD membrane preparation may be found in our previous report (Khayet and Matsuura, 2001).

PV membrane characterization

Contact Angle Studies. Both the advancing and the receding contact angles of water and formamide on the top surface of the prepared PV membranes were measured at room temperature by using a contact angle meter 14-in. Horizontal Beam Comparator (model 22-2000 Series; Scherr-Tumico, St. James, MN). Initial drops of 3 μL were deposited on the membrane surface using a tight syringe that was adjusted 5×10^{-4} m over the membrane surface. The measurements were carried out on each membrane sample at more than 10 different spots and the mean values, together with the standard deviations of both the advancing and the receding contact angles of water and formamide, are reported herein.

Swelling Measurements. The swelling degree of the PV membranes was measured in 1 kg/m^3 chloroform–aqueous solution. The dried membrane was first weighed and then immersed in the chloroform–water mixture for 24 h at 298 K. The membranes were then removed from the vessel, wiped quickly with filter paper to remove the excess solution, and weighed again. The swelling degree (*SD*) was determined from

the ratio of the weight of the swollen membrane to the weight of the dried membrane.

Pervaporation Experiments. PV experiments were conducted using the laboratory system described elsewhere (Khayet and Matsuura, 2001). It consists of a static stainless cell connected to a heating system through its jacket to control the temperature of the liquid feed. The membrane effective area is 9.84×10^{-4} m^2. The total volume of the upper chamber is 381.7×10^{-6} m^3. The temperature was measured inside the cell by a sensor connected to a digital meter with an accuracy of ± 0.1 K. A vacuum pump, which was associated with a vacuum pressure controller, was connected to the permeate side of the cell to remove the vapor and the downstream pressure was measured by a digital pressure transducer with an accuracy of about $\pm 2\%$. Two glass cold traps, filled automatically with liquid nitrogen, were installed to recover the permeate. In all experiments the temperature was maintained at 298 K, the downstream pressure at 1666.5 Pa, the stirring rate was 53.3 rps (maximum stirring), and the initial chloroform concentration in the feed was varied from 1 to 2 kg/m^3.

The mass flux of the membrane was determined, in every case, from the weight of the condensate collected in each trap for a predetermined period of time. The compositions of the feed and permeate were determined using a Varian 3300 gas chromatograph (Varian Associates, Palo Alto, CA), equipped with an Alltech Chemipack® C18, 80/100 Column (Alltech, Guelph, Ontario, Canada). In each experiment, the chloroform concentration in the feed side was measured as a function of time. All experiments were repeated at least two times to ensure reproducibility of the measurements and the separation factor was calculated using the following expression

$$\alpha = \frac{x_{ch,p}/x_{w,p}}{x_{ch,f}/x_{w,f}} \tag{1}$$

where $x_{ch,p}$, $x_{w,p}$, $x_{ch,f}$, and $x_{w,f}$ are the mole fractions of chloroform and water in the permeate and feed, respectively.

MD membrane characterization

In our previous paper (Khayet and Matsuura, 2001) the following MD membrane characteristics were determined.

Membrane porosity, defined as the volume of the pores divided by the total volume of the membrane, was determined by measuring the density of the polymer material using isopropyl alcohol (IPA), which penetrates inside the pores of the membrane and the density of the membrane using pure water, which does not enter the pores.

Membrane liquid entry pressure of water (*LEPw*), which is the pressure that must be applied onto pure water before it penetrates into dried membrane pores, was also measured. This pressure depends on the maximum pore size and on the hydrophobicity of the membrane. It decreases as the pore size increases and/or the contact angle decreases.

The membrane thickness was measured with a digital micrometer on ten spots for each membrane sample and the average values are given in this study.

The average pore size and the effective porosity (defined as the ratio of the porosity and the effective pore length that takes into account the tortuosity of the membrane pores) were determined using the gas permeation method.

The maximum pore size was determined by the bubble-point method and the mean pore size together with the pore size distribution were obtained from the wet and dry flow method. The method suggested by Kesting (1985) was used in our previous study (Khayet and Matsuura, 2001) to obtain the pore size distribution. In this report, another method is proposed in the theoretical section to determine the mean pore size, geometric standard deviation, and pore size distribution.

Finally, VMD experiments were carried out using the same laboratory system used to conduct PV experiments and the operating conditions stated earlier for PV.

The methods and instruments used to carry out these measurements were explained in detail in Khayet and Matsuura (2001).

Theory

Analysis of data on wet and dry flow method: MD membrane pore-size distribution

The wet and dry flow method was used to determine the maximum pore size, the mean pore size, and the pore size distribution. This method has been frequently used to characterize microfiltration and ultrafiltration membranes (Hernández et al., 1996; Nakao, 1994). Gas permeation velocity (J_d) is measured through a dried membrane at 298 K and different transmembrane pressures. Then, the membrane is wetted by IPA and again the permeation velocity (J_w) is measured for different transmembrane pressures. Monitoring the initial flow of gas, the point at which gas is first seen to pass through the sample (that is, the bubble point), allows calculation of the maximum pore size. Increasing the pressure still further allows the gas to flow through smaller pores, according to the Laplace equation. In the wet run, when all the pores are emptied, the pressure flow curve will return to that slope obtained with a dry sample. The two runs (dry and wet curves) allow mean pore size, geometric standard deviation, and pore size distribution to be determined using the following procedure.

The cumulative flow for the pores with sizes below $d_p(j)$, that is, pore in the jth class ($j = 1, \ldots, n$), is

$$g_a(j) = 1 - g'_a(j) = 1 - \frac{J_w(j)}{J_d(j)} \tag{2}$$

The differential flow through pores in the jth class with a pore diameter $d_p(j)$ is

$$g_d(j) = \frac{g'_a(j+1) - g'_a(j-1)}{2} \tag{3}$$

Taking into account that flow is proportional to pore area, the number of pores with size $d_p(j)$ is

$$n_d(j) = K \frac{g_d(j)}{d_p(j)^2} \tag{4}$$

where K is a normalization factor that can be evaluated as

$$K = \frac{g_a(n)}{\sum_{j=1}^{n} g_d(j)/d_p(j)^2} \tag{5}$$

Finally, the cumulative distribution of number of pores is

$$n_a(j) = \sum_{k=1}^{j} n_d(k) \tag{6}$$

As stated in our previous articles (Khayet et al., 2002, 2003), the pore-size distribution can be expressed by the probability density function (that is, log-normal distribution) described by the following equation

$$\frac{df(d_p)}{d(d_p)} = \frac{1}{d_p \ln \sigma_p (2\pi)^{1/2}} \exp\left[- \frac{(\ln d_p - \ln \mu_p)^2}{2(\ln \sigma_p)^2} \right] \tag{7}$$

where d_p is the pore size, μ_p is the mean pore size, and σ_p is the geometric standard deviation. In this study, the function $f(d_p)$ was used to fit the obtained cumulative distribution of relative number of pores $n_a(j)$, and the mean pore size μ_p, together with the geometric standard deviation σ_p, are evaluated for each MD membrane. The mean pore size will correspond to 50% of the cumulative number of pores and the geometric standard deviation can be calculated from the ratio of 84.13% of the cumulative number of pores to that of 50%.

In addition, the surface porosity ε_s, defined as the ratio between the area of the pores to the total membrane surface area, can be calculated from Eq. 8

$$\varepsilon_s = \frac{N\pi}{4} \sum_{j=1}^{n} f_j d_j^2 \tag{8}$$

where N is the number of pores per unit area, known as pore density, and f_j is the fraction of the number of pores with size d_j.

We note here that the surface porosity ε_s is different from the void volume ε, which is determined as (Martínez, 2002)

$$\varepsilon = \varepsilon_s \tau \tag{9}$$

where τ is the pore tortuosity.

Thus, the number of pores per unit area can be calculated from the following equation

$$N = \frac{\varepsilon/\tau}{\sum_{j=1}^{n} f_j \pi r_j^2} \tag{10}$$

if the effective membrane porosity, which takes into account the tortuosity of the membrane pores, ε/τ, is known.

Mass transfer of a single component through membrane pores

Transport of gas through porous media has been extensively studied and theoretical models have been developed based on the kinetic theory of gases (Mason and Maulinaskas, 1983; Matsuura, 1993; Present, 1958). In MD, various types of mechanisms have been proposed for transport of gases or vapors through microporous membranes: Knudsen model, viscous model, ordinary molecular diffusion model, and/or the combination among them, often summarized by the dusty gas model (Lawson and Lloyd, 1997). In our previous works, the physical nature of the mass transport through microporous and hydrophobic membranes was analyzed in DCMD and SGMD processes (Khayet et al., 2000, 2001). In both MD configurations it was concluded that the vapor transport takes place by a combined Knudsen/molecular diffusion mechanism. In the VMD process, the ordinary molecular diffusion resistance is neglected because it is proportional to the partial pressure of air in the membrane pores and in VMD only traces of air are present within the membrane pores. Thus, the VMD mass flux was described by the Knudsen model (Bandini et al., 1997) or combined Knudsen/viscous model (Lawson and Lloyd, 1996), depending on the membrane pore size.

The governing quantity that provides a guideline in determining which mechanism is operative in a given pore under given experimental conditions is the ratio of the pore size to the mean free path λ, which is calculated for a species i using the following expression (Matsuura, 1993; Present, 1958)

$$\lambda_i = \frac{kT}{\sqrt{2}\pi \bar{p} \sigma_i} \tag{11}$$

where σ_i is the collision diameter, k is the Boltzmann constant, $\bar{p}$ is the mean pressure within the membrane pores, and T is the absolute temperature.

Matsuura (1993) stated that Knudsen type flow is predominant when the ratio of the pore radius to the mean free path (that is, r_p/λ) is <0.05. In this case, the molecule–pore wall collisions dominate the gas-transport mechanism and the molar flow rate (mol/s) of component i may be expressed as follows

$$F_i^k = \frac{2\pi}{3} \frac{1}{RT} \left(\frac{8RT}{\pi M_i} \right)^{1/2} \frac{r_k^3}{\tau\delta} (p_{i,m} - p_{i,p}) \tag{12}$$

where r_k is the pore size for Knudsen flow; M_i is the molecular weight of gas i; R is the gas constant; $p_{i,m}$ and $p_{i,p}$ are the partial pressures at the upstream and the downstream of the membrane surface, respectively; δ is the membrane thickness; and τ is the pore tortuosity.

When $(r_p/\lambda) > 50$, the molecule–molecule collisions will dominate and viscous flow occurs (that is, Poisseuille flow). Under this mechanism, the molar flow rate of species i is expressed as

$$F_i^v = \frac{\pi r_v^4}{8\eta_i} \frac{\bar{p}}{RT} \frac{1}{\tau\delta} (p_{i,m} - p_{i,p}) \tag{13}$$

where r_v is the pore radius in the Poisseuille region, η_i is the viscosity of species i, and $\bar{p}$ is the average pressure in the pore.

When the radius r_p is between 0.05 and 50λ, both molecule–molecule and molecule–wall interactions have to be considered and the pores contribute to the total mass transport by a mechanism operative in the Knudsen–viscous transition region. In this case, the molar flow can be described by Eq. 14, as reported by Present (1958), Lawson and Lloyd (1997), and Martínez et al. (2002)

$$F_i^t = \frac{\pi}{RT\tau\delta}\left[\frac{2}{3}\left(\frac{8RT}{\pi M_i}\right)^{1/2} r_t^3 + \frac{r_t^4}{8\eta_i}\bar{p}\right](p_{i,m} - p_{i,p}) \quad (14)$$

where r_t is the pore radius in the transition region.

In the case of a membrane with a distribution of pore size, all the above mechanisms can occur simultaneously, but to different extents, depending on the operating conditions of pressure, temperature, and the gas or vapor under study. Hence, the total mass flow can be estimated by considering each pore by applying the relevant flow equation for mass transfer through it and then summating the flow over the entire system of pores. Therefore, the total mass transport in the gas phase F_i^g is given by

$$F_i^g = \frac{N}{\tau\delta}\left(\sum_{j=1}^{m(r=0.05\lambda)} G_i^k f_j r_j^3 + \sum_{j=m(r=0.05\lambda)}^{p(r=50\lambda)} (G_i^k f_j r_j^3 + G_i^\nu f_j r_j^4 \bar{p}) + \sum_{j=p(r=50\lambda)}^{n(r=r_{max})} G_i^\nu f_j r_j^4 \bar{p}\right)(p_{i,m} - p_{i,p}) \quad (15)$$

where

$$G_i^k = \left(\frac{32\pi}{9M_iRT}\right)^{1/2} \quad (16)$$

$$G_i^\nu = \frac{\pi}{8\eta_i}\frac{1}{RT} \quad (17)$$

and f_j is the fraction of pores with pore radius r_j, N is the total number of pores per unit area as stated earlier, m is the last class of pores in the Knudsen region, and p is the last class of pores in the transition region.

It is to be noted that in Eq. 15 the upper limit of each summation is altered by the relative values of the maximum pore radius (r_{max}). The following three cases are possible: (1) if ($r_{max} < 0.05\lambda$), only Knudsen mechanism prevails; (2) if ($r_{max} < 50\lambda$), the upper limit of transition is r_{max} and both Knudsen and transition mechanisms are applicable; and (3) if ($r_{max} > 50\lambda$) all mechanisms are operative simultaneously.

Mass transfer of a single component through nonporous membrane

In MD processes, a transport of adsorbed molecules or atoms on membrane solid surfaces (that is, surface diffusion) is neglected because of the fact that the diffusion area of the membrane matrix is small compared to the pore area (Lawson and Lloyd, 1997). Thus far, it is considered that the flow of gas or vapor is uninfluenced by the forces of interaction between the compound to be separated and the membrane material. In fact, the possibility of the sorption of component in the polymer and diffusion through the body of the polymer is valid only for the limiting case of transport through nonporous membranes. For hydrophobic membranes, such as those used in MD, the "affinity" between water and the membrane material is very low and it may be allowed to neglect the contribution of transport through the nonporous membrane portion, especially for porous membranes with large pore sizes and high porosities. Nevertheless, the mechanism may have a significant effect once other compounds are present in the feed solution, especially for species that have strong "affinity" with the membrane matrix. In this case, the solution–diffusion mechanism has to be taken into consideration primarily for membranes with low porosity and small pore size.

Based on the solution–diffusion mechanism, the permeation rate of a single component (i) through a dense membrane, in PV, can be described by Fick's first law (Huang, 1991; Zhang and Drioli, 1995)

$$F_i^d = -D_i\frac{dC_i}{dx} \quad (18)$$

where D_i is the diffusion coefficient and C_i is the concentration of the component (i) in the membrane. Accordingly, assuming a uniform concentration gradient, the permeation rate can be described by

$$F_i^d = D_i\frac{C_{i,m} - C_{i,p}}{\delta} \quad (19)$$

where

$$C_{i,m} = S_i p_{i,m} \qquad \text{and} \qquad C_{i,p} = S_i p_{i,p} \quad (20)$$

$C_{i,m}$ and $C_{i,p}$ are the concentrations of the component i; $p_{i,m}$ and $p_{i,p}$ are the vapor pressures in the upstream and downstream of the membrane surface, respectively; and S_i is the solubility coefficient. Thus

$$F_i^d = D_i S_i\frac{p_{i,m} - p_{i,p}}{\delta} = K_i\frac{p_{i,m} - p_{i,p}}{\delta} \quad (21)$$

where $K_i = D_i S_i$ is the membrane permeability.

Finally, the total gas flow as a result of contributions by all the mechanisms may be given by the sum of gas phase flow through the membrane pores (F_i^g) and flow through the nonporous portion (F_i^d)

$$F_i^t = \left[\frac{N}{\tau\delta}\left(\sum_{j=1}^{m(r=0.05\lambda)} G_i^k f_j r_j^3 + \sum_{j=m(r=0.05\lambda)}^{p(r=50\lambda)} (G_i^k f_j r_j^3 + G_i^\nu f_j r_j^4 \bar{p}) + \sum_{j=p(r=50\lambda)}^{n(r=r_{max})} G_i^\nu f_j r_j^4 \bar{p}\right) + \frac{1}{\delta}\left(1 - N\sum_{j=1}^{n} f_j \pi r_j^2\right)K_i\right](p_{i,m} - p_{i,p}) \quad (22)$$

Additionally, it is well known that in VMD, a simultaneous heat and mass transfer through the membrane occurs and the temperature at the vapor–liquid interface differs from the bulk conditions. The heat required for the interfacial evaporation is supplied by the heat flux through the liquid phase, neglecting the heat transfer through the vacuum side. A simple enthalpy balance usually used in the VMD process is (Bandini et al., 1997; Lawson and Lloyd, 1996, 1997)

$$h_f(T_b - T_m) = \sum_{i=1}^{s} F_i^t \Delta H_{v,i} \tag{23}$$

where $\Delta H_{v,i}$ is the evaporation enthalpy of species i of transmembrane flux (F_i^t), s is the number of permeated components, h_f is the heat transfer coefficient in the liquid phase, T_b is the feed bulk temperature, and T_m is the temperature at the liquid–vapor interface.

For pure components, Antoine's equation can be used to calculate the partial pressure at the membrane surface $p_{i,m}$ (Lawson and Lloyd, 1997).

In this work, the heat transfer coefficient is correlated for turbulent liquid flow by the following semiempirical correlation (Lawson and Lloyd, 1996, 1997)

$$\mathrm{Nu} = 0.023\,\mathrm{Re}^{0.8}\mathrm{Pr}^{1/3} \tag{24}$$

where Nu, Re, and Pr are the Nusselt, Reynolds, and Prandtl numbers, respectively.

According to the equations developed above, the prediction of the permeation molar flux of pure component can be performed as follows: First, λ_i is calculated using Eq. 3 and all necessary summations are then evaluated using membrane pore size distribution. Also, the quantities G_i^k and G_i^v, if needed, are evaluated at the bulk feed temperature using Eqs. 16 and 17. The permeability coefficient K_i is obtained from PV experiments using dense PVDF membranes together with Eqs. 21, 23, and 24. With the numerical values generated above, the total molar flux F_i^t, in Eq. 22, is calculated at the feed bulk temperature. Subsequently, the membrane surface temperature T_m is evaluated using Eqs. 23 and 24 and this temperature is used to evaluate second values of G_i^k, G_i^v, and F_i^t. This procedure is repeated until the difference between two successive calculated molar fluxes is less than 0.1%.

Applicable flux equations for a binary organic–water mixture

For a binary mixture, each compound may travel by any of the transport mechanisms cited previously, depending on the pore size it travels through and the absolute pressure in the pore. In the Knudsen regime, transport of molecules is controlled by molecule–wall collisions and the molecules travel independently from each other. In viscous flow, the pore size is much larger than the mean free path of the molecules and molecule–molecule interactions dominate.

In developing flux equations for each component in a binary mixture and for the purpose of simplicity it is assumed that: flow of each species is only one dimensional, the molecules are not adsorbed on the walls of the membrane pores, solution–diffusion mechanism occurs at the defect-free dense membrane surface portion, and the sorption of the individual species on the membrane surfaces is independent.

For gaseous mixtures of two components, the mean free path and the collision diameters are different from the corresponding quantities for the pure component. In this study, the following relationship was applied for organic–water mixtures

$$\sigma_{o-w} = \frac{\sigma_w + \sigma_o}{2} \tag{25}$$

and then λ_{o-w} is calculated from Eq. 11. The subscripts o and w refer to organic and water components, respectively.

With the above assumptions and from Eq. 22, the individual fluxes of the mixture can be written as

$$F_i^t = \frac{N}{\tau\delta}\left(\sum_{j=1}^{m(r=0.05\lambda)} G_i^k f_j r_j^3 \Delta p_i + \sum_{j=m(r=0.05\lambda)}^{p(r=50\lambda)} (G_i^k f_j r_j^3 \Delta p_i + G_i^v f_j r_j^4 \bar{p}_i \Delta p) + \sum_{j=p(r=50\lambda)}^{n(r=r_{max})} G_i^v f_j r_j^4 \bar{p}_i \Delta p\right) + \frac{1}{\delta}\left(1 - N\sum_{j=1}^{n} f_j \pi r_j^2\right) K_i \Delta p_i \tag{26}$$

where Δp is the total pressure difference across the membrane, Δp_i is the partial pressure difference of component i, and $\bar{p}_i$ is the average partial pressure of component i.

For an organic–water binary mixture, the following applicable relationships can be used

$$\Delta p_o = Y_{o,m} p_m - Y_{o,p} p_p \tag{27}$$

$$\Delta p_w = Y_{w,m} p_m - Y_{w,p} p_p \tag{28}$$

$$\bar{p}_o = \frac{Y_{o,m} p_m + Y_{o,p} p_p}{2} \tag{29}$$

$$\bar{p}_w = \frac{Y_{w,m} p_m + Y_{w,p} p_p}{2} \tag{30}$$

$$Y_{o,m} + Y_{w,m} = 1 \tag{31}$$

and

$$Y_{o,p} + Y_{w,p} = 1 \tag{32}$$

where Y is the mole fraction in the vapor phase of each species. The subscripts w and o refer to water and organic components, respectively, whereas m and p indicate feed membrane surface and permeate, respectively.

Consequently, from the above equations

$$\Delta p = \Delta p_o + \Delta p_w = p_m - p_p \tag{33}$$

Moreover, the mole fractions of organic and water in the permeate can be written as

$$Y_{o,p} = \frac{F_o^t}{F_o^t + F_w^t} \tag{34}$$

$$Y_{w,p} = \frac{F_w^t}{F_o^t + F_w^t} \tag{35}$$

Rewriting the above Eq. 34 and substituting for F_o^t and F_w^t using Eqs. 26 to 33, we obtain the following quadratic equation in terms of $Y_{o,p}$ after appropriate simplifications

$$\begin{aligned}
&\Bigg[(G_w^k - G_o^k)I_1 p_p + (K_w - K_o)I_3 p_p \\
&\qquad + \frac{1}{2}(G_o^k - G_w^k)I_2(p_m - p_p)p_p\Bigg]Y_{o,p}^2 \\
&+ \Bigg[(G_o^k I_1 + K_o I_3)Y_{o,m}p_m + (G_w^k I_1 + K_w I_3)Y_{w,m}p_m \\
&\qquad + \frac{1}{2}G_o^v I_2(p_m - p_p)(Y_{o,m}p_m - p_p) \\
&\qquad + \frac{1}{2}G_w^v I_2(p_m - p_p)(Y_{w,m}p_m + p_p) \\
&\qquad + (G_o^k - G_w^k)I_1 p_p + (K_o - K_w)I_3 p_p\Bigg]Y_{o,p} \\
&- (G_o^k I_1 + K_o I_3)Y_{o,m}p_m - \frac{1}{2}G_o^v I_2(p_m - p_p)Y_{o,m}p_m = 0
\end{aligned} \tag{36}$$

where

$$I_1 = \frac{N}{\tau\delta}\sum_{j=1}^{p(r=50\lambda)} f_j r_j^3 \tag{37}$$

$$I_2 = \frac{N}{\tau\delta}\sum_{j=m(r=0.05\lambda)}^{n(r=r_{max})} f_j r_j^4 \tag{38}$$

$$I_3 = \frac{1}{\delta} - \frac{N}{\delta}\sum_{j=1}^{n(r=r_{max})} f_j \pi r_j^2 \tag{39}$$

For dilute organic aqueous mixture, the partial pressure of the organic compound ($Y_{o,m}p_m$) was estimated using Henry's law, whereas that of water ($Y_{w,m}p_m$) was evaluated from Raoult's law (Urtiaga et al., 1999, 2000, 2001).

Moreover, as stated earlier, heat and mass transfer occur simultaneously and both concentration and temperature polarization take place in the liquid phase. In VMD and hydrophobic PV processes, the organic mole fraction at the interface is smaller than the corresponding bulk value and, consequently, the mole fraction of water at the interface is larger than that in the bulk. The mass transfer through the liquid phase can be adequately described by the film theory model and the mole fraction in the liquid bulk ($x_{i,b}$) and at the interface ($x_{i,m}$) are related to the molar fluxes by the following relationship (Lawson and Lloyd, 1996):

$$x_{i,m} = x_{i,p} + (x_{i,b} - x_{i,p})\exp\left(\frac{F^t}{k_l C_l}\right) \tag{40}$$

where F^t is the total molar flux, C_l is the bulk molar concentration in the liquid phase, $x_{i,p}$ is the mole fraction in the permeate, and k_l is the mass transfer coefficient given by the mass transfer analogy of Eq. 24 (Lawson and Lloyd, 1997)

$$\mathrm{Sh} = 0.023\,\mathrm{Re}^{0.8}\mathrm{Sc}^{1/3} \tag{41}$$

where Sh and Sc are the Sherwood and Schmidt numbers, respectively.

The Wilke–Chang correlation (Wilke and Chang, 1955) was used to calculate the value of the ordinary diffusion coefficient of organic in water and, for dilute organic aqueous mixture, it was considered that the physical properties of pure water were applicable.

Finally, the prediction of separation factor, together with the organic and water permeation molar fluxes, can be performed following the steps indicated below: Initially, λ_{o-w} is calculated using Eqs. 11 and 25 and the summations I_1, I_2, and I_3 are evaluated from Eq. 37 to Eq. 39. G_i^k and G_i^v are then evaluated at the bulk feed temperature using Eqs. 16 and 17, respectively. For dilute organic aqueous mixture, the viscosity of pure water was considered. The values of the permeability coefficients K_o and K_w are obtained by pervaporation experiments. With the numerical values generated above, Eq. 36 is solved in terms of $Y_{o,p}$. Subsequently, the molar flux of each specie, F_i^t, is calculated using Eq. 26 and then both temperature and composition at the membrane surface are calculated by means of Eqs. 23, 24, 40, and 41. The quantities G_i^k and G_i^v are evaluated again taking into account both the temperature and concentration polarization effects and second values of the molar flux of each species is obtained. The procedures are repeated until the difference between two successive calculated molar fluxes is less than 0.1%. The experimental fluxes are then compared to the calculated values.

Results and Discussion

Results on morphological characterization of MD membranes

The liquid entry pressure of water (*LEPw*), porosity, pore size, and effective porosity of the MD membranes were measured as described in our previous paper (Khayet and Matsuura, 2001). Table 1 lists the characteristics of the MD membranes used herein. It was found that the effect of pure water as an additive in the PVDF casting solution is to increase both the pore size and the porosity of the prepared membranes. The membrane *LEPw* decreases as the concentration of water in the PVDF casting solution increases. This is attributed to the increase of the maximum pore size of the membranes.

Some results obtained for air flow through MD membranes, when they are dry and when they are wetted by isopropyl alcohol, were presented elsewhere (Khayet and Matsuura, 2001). In Figures 2a and b, the cumulative pore size distribu-

Table 1. MD Membrane Characteristics: Membrane Thickness (δ), Liquid Entry Pressure of Water (*LEPw*), Porosity (ε), Mean Pore Size (μ_p), Effective Porosity (ε/L_p), Geometric Standard Deviation (σ_p)

					Gas Permeation Test		Log-Normal Function	
Membrane	H_2O* (wt %)	δ (μm)	*LEPw* (10^5 Pa)	ε (%)	μ_p (nm)	ε/L_p (m^{-1})	μ_p (nm)	σ_p
W0	0	50.7	28.96	26.8	10.88	4363.4	11.09	1.10
W1	0.85	50.2	25.10	31.6	19.85	4559.4	20.03	1.05
W2	1.70	53.1	16.89	40.1	29.90	5949.3	29.68	1.07
W3	2.55	49.8	13.79	33.6	41.67	6191.8	40.96	1.04
W4	3.40	52.8	7.10	48.3	59.20	6728.9	58.31	1.08
W5	4.25	50.6	6.34	52.6	99.48	7878.1	99.11	1.10
W6	5.10	61.8	1.52	70.5	220.30	7505.5	225.82	1.18

*Water content in casting solution in (wt %) and for all membranes; PVDF concentration is 15 wt %.

tion data obtained from Eqs. 2 to 6 are shown together with the fitting curves to the log-normal distribution function. It can be observed that the pore size distribution curves were shifted to the right as the water content in the PVDF casting solution was increased. The mean pore size (μ_p) and the geometric standard deviation (σ_p) were calculated as stated earlier. The results are also given in Table 1. The pore size determined from the fitting to the log-normal distribution function agrees well with that obtained from the gas permeation test. The probability density function curves were also generated from Eq. 7 and are presented in Figures 3a and b. As shown, there is a rightward shift of the probability density function curve for the membranes prepared with higher water content in the polymer solution and the pore size distribution becomes lower and narrower around the mean pore size as the water content in the PVDF casting solution decreases.

In addition, the values of the geometrical standard deviation σ_p were very close to each other, varying from 1.04 to 1.18. This indicates, as stated by Michaels et al. (1971), that virtually all the MD membranes were similar in structure. For PVDF hollow-fiber ultrafiltration membranes, values of σ_p between 1.10 and 1.42 were reported by Khayet et al. (2002).

Surface porosity and pore density were calculated from Eqs. 8 and 10, respectively. The results are summarized in Table 2

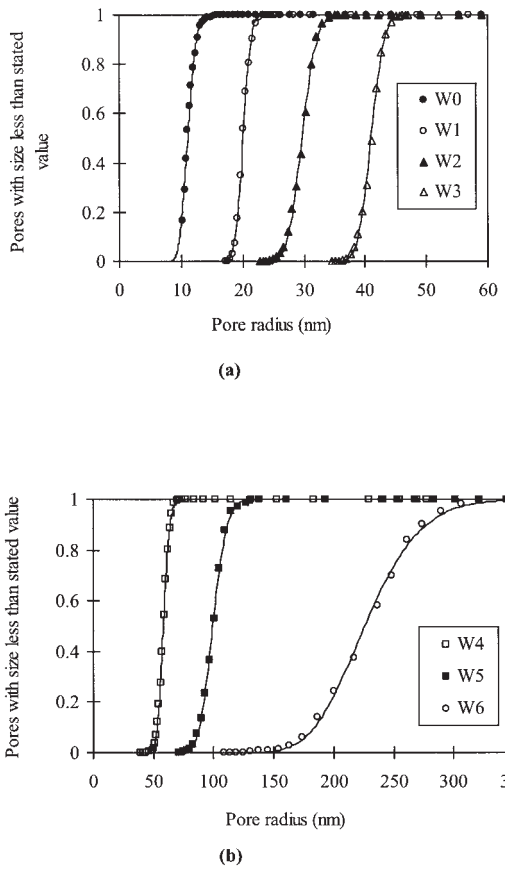

Figure 2. Cumulative pore size distributions of MD membranes.

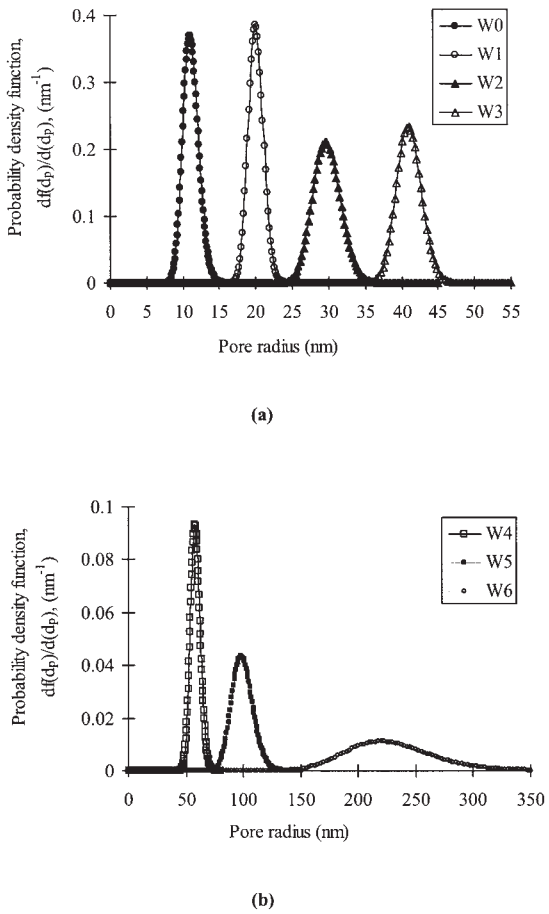

Figure 3. Probability density function curves of MD membranes.

Table 2. MD Membrane Characteristics: Pore Density (N), Surface Porosity (ε_s), Pore Tortuosity (τ)

Membrane	H_2O* (wt %)	N (pores/μm^2)	ε_s (%)	τ
W0	0	557.0	22.12	1.21
W1	0.85	179.0	22.89	1.38
W2	1.70	112.4	31.59	1.27
W3	2.55	57.9	30.84	1.09
W4	3.40	32.7	35.53	1.36
W5	4.25	12.6	39.86	1.32
W6	5.10	2.7	46.38	1.52

*Water content in casting solution in (wt %) and for all membranes; PVDF concentration is 15 wt %.

together with the evaluated pore tortuosity from the effective membrane porosity (ε/L_p). As expected, the pore density decreases with the concentration of water in the PVDF casting solution, whereas the porosity increases. It can be seen that the W0 membrane has the highest pore density. The calculated membrane pore tortuosity was between 1.1 and 1.5. In MD studies, a value of 2 is frequently assumed (Phattaranawik et al., 2002; Schofield et al., 1990; Urtiaga et al., 2000).

Characteristics of PV membranes

The relative wetability of the PVDF membrane surface was studied by measuring both the advancing and the receding contact angles of water and formamide on dense PVDF membranes. The advancing water contact angle is more closely related to the hydrophobic part of a surface, whereas the receding contact angle can be interpreted as the degree of molecular reorientation required to establish a new equilibrium state with the aqueous environment. It was found that both the advancing and receding contact angles of PVDF membranes did not change significantly. For water, the advancing and the receding contact angles remain around values of 82.3 ± 2.1 and 75.2 ± 2.0°, respectively, whereas those of formamide were 68.4 ± 1.8 and 57.7 ± 1.4°, respectively. In fact, PVDF is known as a chemically inert "hydrophobic" fluoropolymer. However, the reported values of the contact angles of PVDF film surfaces are lower than 90°. Owens and Wendent (1969) presented a value of 82°; Huang et al. (2000) obtained a value of 75°; and Nunes and Peinemann (1992) reported a value of 80°. The obtained water contact angles for the PVDF membrane were lower than the measured ones for polytetrafluoroethylene (Teflon; 116° for the advancing contact angle and 92° for the receding contact angle).

Furthermore, the solubility parameter (δ_m) and the surface free energy (γ_m) of the PVDF membrane were estimated from the values of the contact angles as follows.

δ_m is an indicator for the hydrophobicity of a polymer surface and was written as a function of the cohesion energy density of the membrane surface (e_{coh}; Pinnau and Freeman, 2000; Van Krevelen, 1990)

$$\delta_m = (e_{coh})^{1/2} \tag{42}$$

The cohesion energy density can be determined from the surface free energy (γ_m) by using the following equation

$$\gamma_m = 0.75(e_{coh})^{2/3} \tag{43}$$

and γ_m can be calculated from the contact angle measurements of two liquids using the following two equations according to Khayet et al. (2003), Owens and Wendent (1969), and Pinnau and Freeman (2000)

$$\left(1 + \frac{\cos\theta_a + \cos\theta_r}{2}\right)\gamma_l = 2(\gamma_m^d \gamma_l^d)^{1/2} + (\gamma_m^{nd}\gamma_l^{nd})^{1/2} \tag{44}$$

$$\gamma_m = \gamma_m^d + \gamma_m^{nd} \tag{45}$$

where θ_a and θ_r are the advancing contact angle and the receding contact angle, respectively; γ_l is the surface free energies of the liquid; and the superscripts d and nd correspond to the dispersive and nondispersive contributions to the total surface energy, respectively. The adopted values of γ_l, γ_l^d, and γ_l^{nd} for water were 72.8×10^{-3}, 21.8×10^{-3}, and 51.0×10^{-3} J/m^2, respectively; whereas for formamide those values were 58.2×10^{-3}, 39.5×10^{-3}, and 19.0×10^{-3} J/m^2, respectively (Van Krevelen, 1990). It must be pointed out that in Eq. 42, to obtain a value of e_{coh} in 10^6 J/m^3, the value of γ_m must be in mJ/m^2. The obtained values of γ_m, e_{coh}, and δ_m are 30.49×10^{-3} J/m^2, 259.25×10^6 J/m^3, and 16.10×10^3 J$^{1/2}$/m$^{3/2}$, respectively.

It must be pointed out that the estimated value of the solubility parameter of PVDF material from the group contribution using the method of Hoftyzer and Van Krevelen is 15.7×10^3 J$^{1/2}$/m$^{3/2}$ (Van Krevelen, 1990). This value is very close to the above calculated value of 16.1×10^3 J$^{1/2}$/m$^{3/2}$. In contrast, a higher solubility parameter for PVDF (that is, 23.2×10^3 J$^{1/2}$/m$^{3/2}$) was assumed by Bottino et al. (1988). This high value was obtained from the highest limiting viscosity number that corresponds to hexamethylphosphoramide.

It must be mentioned that the solubility parameter of water is 47.9×10^3 J$^{1/2}$/m$^{3/2}$, whereas that of chloroform, 19.0×10^3 J$^{1/2}$/m$^{3/2}$, is closer to the solubility parameter of PVDF. The "affinity" between the polymer and the solvent can be expressed in terms of the interaction parameter $\chi_{i,m}$, which can be calculated from the following expression (Pinnau and Freeman, 2000; Van Krevelen, 1990)

$$\chi_{i,m} = \frac{v_m}{RT}(\delta_m - \delta_i)^2 + 0.34 \tag{46}$$

where R is the gas constant; T is the absolute temperature; v_m is the molar volume of polymer repeat unit; and δ_i and δ_m are the solubility parameters of component i and polymer, respectively.

As the interaction parameter between the polymer and the solvent increases, the amount of liquid inside the polymer membrane increases and $\chi_{i,m}$ decreases. In our case, the calculated interaction parameter between chloroform and PVDF is 0.47, whereas that between water and PVDF is 15.0. Therefore, PVDF membranes have a stronger "affinity" for chloroform than for water. In the pervaporation system and swelling experiments discussed in this work, chloroform is the minor component and water is the major component that is more preferentially repelled by the membranes. This demonstrates why the measured degree of swelling of the PV membranes is

Table 3. Results of Pure Water VMD and PV Experiments

PV			VMD			
δ (μm)	Water Flux (10^{-3} kg m^{-2} s^{-1})	Normalized Water Flux (10^{-9} kg m^{-1} s^{-1})	Membrane	δ (μm)	Water Flux (10^{-3} kg m^{-2} s^{-1})	Normalized Water Flux (10^{-9} kg m^{-1} s^{-1})
38.81	0.16	6.29	W0	50.7	0.19	9.58
49.77	0.13	6.62	W1	50.2	0.35	17.57
59.70	0.11	6.63	W2	53.1	0.65	34.37
83.15	0.08	6.40	W3	49.8	0.93	46.20
110.77	0.06	6.54	W4	52.8	1.44	76.12
			W5	50.6	2.58	130.44
			W6	61.8	4.78	295.44

found to be very low (1.031–1.044 kg/kg). Therefore, most likely, the membrane morphology did not change during pervaporation and the chloroform permeability may be independent of swelling behavior.

Pure water PV and VMD experiments

Similar sets of permeation experiments were conducted using the prepared PV membranes with different thicknesses and MD membranes with different pore sizes. The first experiments were carried out using pure water as feed and the permeated flux was measured at feed temperatures of 298 K, stirring rate of 53.3 revolutions/s (rps), and downstream pressure of 1666.5 Pa. The effects of stirring rate, feed temperature, and downstream pressure in VMD and PV systems were well investigated in a number of studies (Bandini et al., 1997; Huang, 1991; Laganà et al., 2000; Lawson and Lloyd, 1997; Matsuura, 1993; Urtiaga et al., 2000). It must pointed out that the permeate pressure must be lower than the saturation pressure of the feed solution to drive the vapor through the membrane.

The obtained PV water flux and VMD water flux are reported in Table 3. As expected, the PV flux decreases with the membrane thickness (Eq. 21). To compare the permeability of membranes with different thicknesses, the normalized flux was used. It was found that the normalized flux is almost similar for all PV membranes and is 1.5 to 45.5 times higher in the VMD than in the PV process, depending on the MD membrane pore size and porosity. In effect, the VMD flux increases exponentially with the concentration of water in the PVDF casting solution (Khayet and Matsuura, 2001).

Under the experimental conditions used in this work, the calculated mean free path of water vapor λ_w is 5.524 μm. Thus, the membranes having pores whose size is $<$0.5524 μm lend themselves to the Knudsen region. All pores having size between 552.4 μm and the maximum pore size are in the viscous region, and pores in the intermediate range (0.5524 and 552.4 μm) are considered in the transition region. For the MD membranes prepared in this study, all the membranes, except the W6 membrane, have pore size distributions in the Knudsen region. For the W6 membrane, the calculated fraction of pores in the Knudsen region (from Figures 2b and 3b) is 88.85%, whereas only 11.15% is in the transition region. In other words, the average fraction of pore area in the transition region is 18.53%. This means that the majority of membrane area (81.47%) is occupied by the Knudsen region.

Using the theoretical model presented in the previous section for a single component, the theoretical VMD flux was calculated and plotted in Figure 4 together with the experimental flux as a function of the water content in the PVDF casting solution used for the preparation of the MD membranes. The pore size distributions given in Figures 1 and 2 were used in this calculation. Agreement between the experimental and the predicted VMD fluxes is excellent. It is worth noticing that the contribution to the total flux of the solution–diffusion flux through the nonporous portion of the MD membranes decreased from 30.4% for the W0 membrane to 0.3% for the W6 membrane. This is attributed to the fact that the W0 membrane has a lower pore size and porosity. Commercial membranes used in MD have a pore size and porosity that are almost identical to those of W5 and W6 membranes. For these last membranes the solution–diffusion contribution may be neglected (that is, contribution $<$ 1.4%). Furthermore, for the W6 membrane the viscous contribution in the transition region to the total flux is very low (3.2×10^{-3} %). Therefore, under our experimental conditions, Eq. 22 for single gas permeation may be modified, neglecting the viscous contribution in the transition region. The theoretical fluxes of the W5 and W6 membranes were estimated using only the Knudsen model and a good agreement between the experimental and theoretical values was found (that is, the discrepancy between the experimental and the predicted fluxes was 1.8% for the W5 membrane and 1.6% for the W6 membrane). Consequently, this result corroborates the use of the Knudsen mechanism in a previous paper (Bandini et al., 1997) when flat-sheet polytetrafluoroethylene (PTFE, TF200) membrane and polypropylene tubular membrane (Accurel Q3/2) with pore size 0.2 μm and porosities of 60 and 75% were used.

Additionally, the effects of pore size distribution on VMD flux was examined by comparing the mass flux calculated by

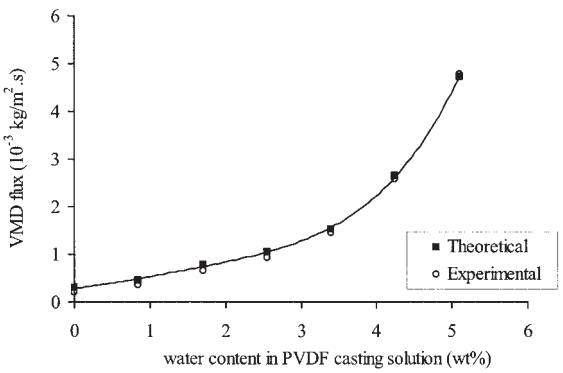

Figure 4. Experimental and simulated VMD flux vs. water content in the PVDF casting solution.

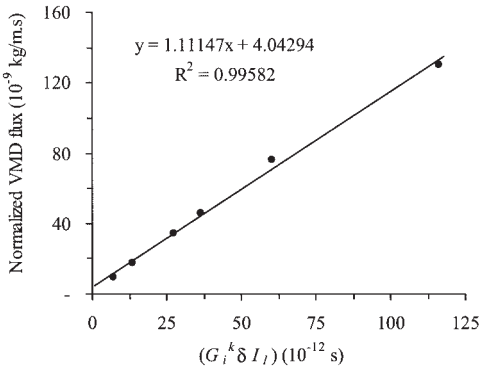

Figure 5. Normalized water flux vs. ($G_i^k \delta I_1$) of the MD membranes.

using Eq. 22 with that obtained by considering the mean values of pore size and porosity. It was found that the fluxes calculated by including the effect of pore size distribution were slightly higher than those calculated from the mean values of pore size and porosity (that is, 0.6 to 4.4%).

As has been well established, the VMD flux depends on membrane thickness, pore size, and effective porosity. Based on Eq. 22, the normalized permeation flux was plotted in Figure 5 as function of the product ($G_i^k \delta I_1$). A linear dependency was observed with reasonably high correlation coefficient ($R^2 = 0.996$). From the intercept of the line, the normalized solution–diffusion flux through the nonporous portion of each MD membrane may be estimated, as shown in Eq. 22. The resulting values lie between 5.2×10^{-9} and 6.7×10^{-9} kg m^{-1} s^{-1}, which are in accordance with the experimental PV normalized fluxes given in Table 3. Moreover, from the slope of the line, as indicated in Eq. 22, the transmembrane pressure ($p_{im} - p_{ip}$) can be determined. A value of 1111.5 Pa was obtained. From this value the temperature of the feed at the membrane surface (T_m) was evaluated using Antoine's equation (Lawson and Lloyd, 1997). A value of 296 K was found, which is lower than the bulk feed temperature (298 K), and is attributed to the temperature polarization effect as stated earlier.

To be more rigorous, for each membrane the simulation program provides an estimated value of the temperature at the membrane surface (T_m), and then the temperature polarization coefficient θ, defined in Eq. 47, was calculated

$$\theta = \frac{T_m - T_{sat}}{T_f - T_{sat}} \tag{47}$$

where T_f is the bulk feed temperature, T_m is the temperature at the feed membrane surface, and T_{sat} is the equilibrium temperature of the feed that corresponds to the pressure on the permeate side.

For systems limited by mass transfer through the membrane, θ values will approach unity. On the contrary, θ values approach zero for systems that are limited by heat transfer to the membrane surface (Bandini et al., 1997; Lawson and Lloyd, 1996). In our case, the temperature polarization coefficients decrease from 0.98 to 0.67 as the membrane permeability (that is, pore size and porosity) increases.

It is worth noting that the estimated values of the heat transfer coefficient increased from 3405.5 for the W0 membrane to 3438.4 W m^{-2} K^{-1} for the W6 membrane. The MD literature values reported a range from 3,000 to 10,000 W $m^{-2} \cdot K^{-1}$ (Lawson and Lloyd, 1996, 1997). We must mention that the heat-transfer correlation used in this study (Eq. 24) does not take into account the mass transport through the membrane and the applicability of this equation in MD system must be investigated (Mengual et al., 2001). This fact will be discussed later with respect to the mass-transfer analogy, Eq. 41.

Chloroform/water PV and VMD experiments

PV and VMD experiments were carried out using PV membranes with different thicknesses and VMD membranes having different pore sizes. The permeate pressure was held constant at 1666.5 Pa, the feed temperature was 298 K, the stirring rate was 53.3 rps (maximum stirring), and the initial chloroform concentration in the feed side was about 1 kg/m^3. The experimental results including separation factor and chloroform and water permeate fluxes are summarized in Table 4. It must be pointed out that, because of the decrease of the chloroform concentration in the feed side (that is, from 37.4 to 63.6%), the presented values of the separation factor refer to the mean value obtained from the beginning to the end of the experiment. As can be seen, under the same experimental conditions, the separation factor of the MD membranes decreases with an increase in the concentration of water in the PVDF casting solution and the separation factor is higher for the PV membranes. This means that the chloroform enrichment in the permeate side is higher using dense PVDF membranes and MD with lower pore size and porosity. Furthermore, it appears that the chloroform/water selectivity of the PV membranes increases with increasing membrane thickness. In fact, the selectivity of the PV membranes is associated not only with the surface characteristics but also with the diffusion through the

Table 4. Results of the Chloroform/Water VMD and PV Experiments

PV				VMD			
δ (μm)	Water Flux (10^{-4} kg m^{-2} s^{-1})	Organic Flux (10^{-5} kg m^{-2} s^{-1})	α*	Membrane	Water Flux (10^{-4} kg m^{-2} s^{-1})	Organic Flux (10^{-5} kg m^{-2} s^{-1})	α*
38.81	1.69	2.47	146.02	W0	1.66	1.20	72.45
49.77	1.28	1.81	141.69	W1	3.21	1.45	45.23
59.70	1.17	1.91	163.15	W2	6.13	2.14	34.91
83.15	0.87	1.40	160.47	W3	8.37	2.48	29.63
110.77	0.66	1.14	173.32	W4	13.59	2.56	18.85
				W5	24.61	3.18	12.93
				W6	44.25	3.49	7.89

*Mean value of the separation factor from the beginning to the end of the experiment.

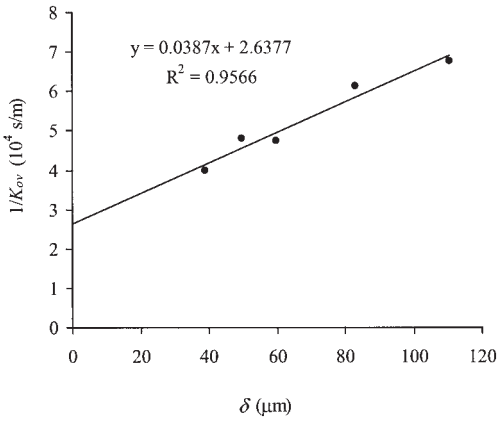

Figure 6. Reciprocal of the overall mass transfer coefficient of the PV membrane as a function of the membrane thickness.

membrane bulk structure. Linear relationships can be plotted between the PV fluxes (that is, chloroform, water, and total fluxes) and the reciprocal of the membrane thickness as predicted by the solution–diffusion model (Eq. 21) and the membrane permeabilities may be calculated.

Moreover, to study the effect of the initial concentration in the feed solution, further PV experiments were carried out using three different initial concentrations (that is, 1, 1.5, and 2 kg/m^3), whereas all the other operating conditions were maintained the same as those mentioned previously. In each experimental run, a decrease in the chloroform concentration on the feed side was observed. The plot of the logarithmic ratio of the initial feed concentration and the concentration at certain time [that is, $\ln(C_0/C)$] vs. operation time is linear and the slope depends on the PV membrane used. A similar behavior was observed when using MD membranes, as stated in our previous article (Khayet and Matsuura, 2001). This indicates that the change of dimensionless concentration with time does not depend on the initial concentration C_0. The same results were observed in other studies (Gronda et al., 2000; Hickey and Gooding, 1994; Urtiaga et al., 1999, 2000, 2001). In this case, the overall mass-transfer coefficient K_{ov} can be determined using Eq. 48, as indicated by Hickey and Gooding (1994), Urtiaga et al. (1999), Khayet and Matsuura (2001), and Gronda et al. (2000)

$$K_{ov} = \frac{V}{At} \ln\left(\frac{C_0}{C}\right) \tag{48}$$

where V is the initial volume of the liquid in the feed side and A is the membrane area.

Figure 6 shows the reciprocal of the obtained K_{ov} values of the PV membranes as a function of the membrane thickness. As can be observed the data may be fitted by a straight line, with a correlation coefficient of 0.96. From the resistances in series model, by assuming negligible resistance in the permeate side at a downstream pressure as low as 1666.5 Pa for flat-sheet membranes the overall resistance may be considered to be a sum of the resistances of the liquid film and membrane, as stated in Hickey and Gooding (1994) and Gronda et al. (2000).

$$\frac{1}{K_{ov}} = \frac{1}{k_l} + \frac{\delta}{HK_o} \tag{49}$$

where k_l is the mass-transfer coefficient in the liquid phase, δ is the membrane thickness, K_o is the membrane permeability, and H is the Henry's law coefficient. For a dilute chloroform–aqueous mixture, the variation of Henry's law constant is an exponential function of temperature (Leighton, 1981; Urtiaga et al. 2000).

Thus, from Eq. 49 the slope of the data in Figure 6 is the inverse of the pervaporation permeability, whereas the intercept is the resistance of the liquid feed boundary layer k_l^{-1}. The obtained PV membrane permeability is 2.0×10^{-10} mol s^{-1} kg^{-1}, whereas the value of k_l is 3.79×10^{-5} m/s. This last value is almost similar to that determined in our previous article when using MD membranes (that is, 3.30×10^{-5} m/s) and the calculated values from the correlation for mass transfer (Eq. 41; that is, 3.11×10^{-5} to 3.19×10^{-5} m/s) (Khayet and Matsuura, 2001). In fact, k_l depends on the hydrodynamic aspect in the feed side of the membrane cell, as was investigated in other studies (Bandini et al., 1997; Gronda et al., 2000; Khayet and Matsuura, 2001; Lawson and Lloyd, 1996; Urtiaga et al., 1999, 2000, 2001). This confirms that the used heat and mass transfer empirical equations can be applicable in our system.

The effect of the boundary layer resistance can be isolated and the membrane resistance to organic mass transfer was calculated. It was found that the resistance of PV membranes with thickness < 60 μm was lower than the liquid boundary layer resistance; and for membranes with similar thickness, as the membrane pore size and porosity increase, the liquid boundary layer resistance becomes the dominating term with respect to the membrane resistance. It must be pointed out that the contribution of the W5 and W6 membrane resistance to the overall resistance is negligible (that is, $<1.7\%$). In contrast, the contribution of the PV membrane resistance to the overall resistance increases from 33.6 to 61.0% as the membrane thickness increases.

In dilute aqueous organic mixtures, because water is abundant in the feed, there is no resistance to water in the liquid phase. Thus, a different procedure is needed to compare the resistances offered by the membrane and by the liquid feed. This fact will be discussed later based on the overall polarization coefficient of water.

The next step in this study was to evaluate the accuracy of the theoretical model presented earlier to predict the performance of chloroform–water VMD application. A simulation program was built using the theoretical procedure given earlier. It must be pointed out that the calculated mean free path, λ_{o-w}, of a chloroform–water mixture under our experimental conditions is 2.388 μm. Therefore, only the W5 and W6 membranes have pore size distributions in the Knudsen and transition regions, whereas the other MD membranes have all pores in the Knudsen region. The fraction of pores in the Knudsen region is 97.7% for the W5 membrane, whereas it is very low for the W6 membrane (2.76×10^{-3} %).

On the other hand, as the chloroform concentration in the feed side decreases with time, for each membrane the theoretical permeate mole fractions together with the organic, water, and total fluxes were determined as function of time and a

mean value was then calculated. It was found that the chloroform flux and selectivity decrease with time, whereas the water flux was maintained practically constant. For example, for the W0 membrane, when the feed chloroform concentration decreased from 1011.5×10^{-3} to 633.15×10^{-3} kg/m^3 (a decrease of 37.4%) in an operation time of about 10,800 s, the calculated chloroform flux decreased by about 38.2% and the water flux decreased only 0.9%. Moreover, as expected, both water and chloroform fluxes increase with the increase of membrane pore size and porosity. In Figure 7 the calculated total fluxes are compared with the experimental data. For all membranes, the predicted total flux is higher than the experimental flux. As was observed when water was used as feed, the viscous contribution in the transition region to the total flux is small for both W5 and W6 membranes (that is, 3.2×10^{-4} % for the W5 membrane and 1.08×10^{-2} % for the W6 membrane). The solution–diffusion contribution to the total organic flux decreased from 40.1 to 0.7% as the membrane pore size and porosity were increased. For water, the solution–diffusion contribution is lower, decreasing from 30.3 to 0.4%.

In Figure 8, the predicted permeate concentration, the experimental permeate concentration, the vapor equilibrium concentration with the bulk feed solution, and the vapor equilibrium concentration obtained from the feed concentration at the membrane surface are plotted as a function of the membrane pore size. It can be observed that the upper limit for the permeate composition is represented by the liquid–vapor equilibrium corresponding to the bulk feed composition and the concentration polarization leads to solute interfacial concentration lower than the bulk concentration. The effect of the concentration polarization is more pronounced at high pore size and porosity. The membrane resistance leads to permeate chloroform content lower than the equilibrium value corresponding to the interfacial conditions at the feed membrane surface. As shown earlier, it can be seen in Figure 8 that the membrane resistance decreases with the increase of the pore size and porosity and the liquid boundary layer resistance in the feed side becomes the dominating resistance. Moreover, the simulated and experimental data have the same tendency; however, the model overestimates the permeate concentration. The discrepancy between the experimental and simulation results can be attributed primarily to the experimental errors, which may have resulted in decreased chloroform fluxes because of its

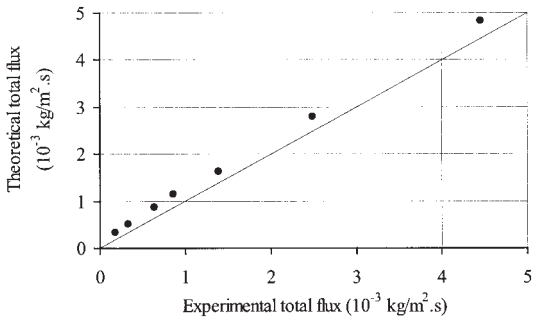

Figure 7. Comparison between the predicted and measured values of the total flux when using chloroform/water mixture.

Temperature, 298 K; downstream pressure, 1666.5 Pa; stirring rate, 53.3 rps; initial chloroform concentration $\approx$ 1 kg/m^3.

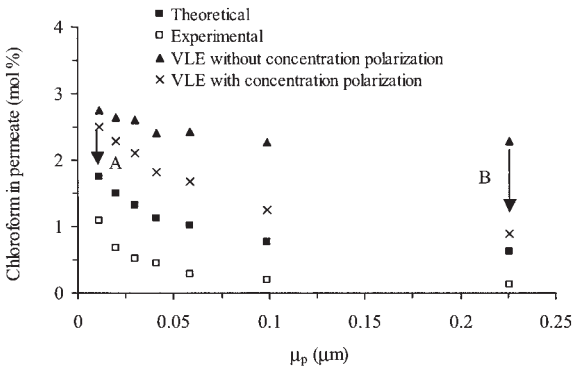

Figure 8. Experimental permeate concentration compared with the simulated one and the vapor–liquid concentrations in equilibrium with the feed solution vs. the membrane mean pore size.

(A) Membrane resistance effect. (B) Concentration polarization effect. Pervaporation experiments: feed temperature, 298 K; permeate pressure, 1666.5 Pa; stirring rate, 53.3 rps (maximum stirring); initial chloroform concentration $\approx$ 1 kg/m^3.

high volatility. At 298 K, the vapor pressure of chloroform is 8.3 times larger than that of water.

As observed, because evaporation takes place at the membrane pore entries, heat and mass transfer resistances through the liquid phase also affect the process selectivity. This phenomenon is a result of the concentration polarization, which lowers the chloroform concentration at the membrane surface. This effect significantly reduces the concentration of chloroform in the permeate. In this study, the overall polarization coefficient for the component i (θ_i) is defined as the ratio between the actual driving force for mass transport across the membrane, resulting from the transport resistances in the liquid feed, and the corresponding maximum value that would be obtained when the transport resistances in the liquid phase are negligible

$$\theta_i = \frac{P_i(T_m, x_{i,m}) - Y_{i,p}P_p}{P_i(T_b, x_{i,b}) - Y_{i,p}P_p} \tag{50}$$

Figure 9 shows the polarization coefficient of water and chloroform as function of the membrane pore size. As can be observed, the polarization effect is higher for the organic compound and when membranes with large pore size (that is, higher permeability) are used. For water, the coefficient θ_w is essentially affected by changes in temperature, given that typically $x_{w,b}$ is very close to $x_{w,m}$. In other words, the mass-transfer resistance in the liquid phase has negligible effects on the water flux.

Conclusions

Polyvinylidene fluoride (PVDF) flat-sheet membranes were used to compare two separation processes: pervaporation (PV) and vacuum membrane distillation (VMD). The prepared MD membranes possessed various pore sizes and a wide range of porosity, whereas the PV membranes were prepared with different thicknesses.

Pure water and dilute aqueous chloroform solutions were

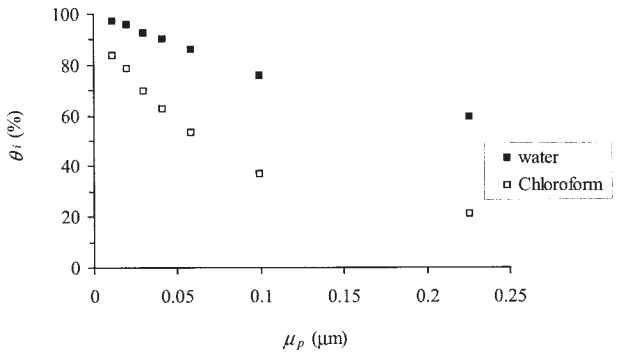

Figure 9. Overall polarization coefficients of water and chloroform vs. the membrane mean pore size.

Pervaporation experiments: feed temperature, 298 K; permeate pressure, 1666.5 Pa; stirring rate, 53.3 rps (maximum stirring); initial chloroform concentration $\approx$ 1 kg/m^3.

used as feed for the permeation experiments. It was found that the mass flux is higher for VMD, whereas the chloroform/water selectivity is higher for the PV membranes and decreases with an increase in the pore size and porosity.

The pore size distributions of the MD membranes were generated from the fitting of the log-normal distribution function to the experimental data obtained from the wet/dry flow method. A good agreement was found between the mean pore size determined from the log-normal distribution function and that evaluated from the gas permeation test.

The water and formamide advancing and receding contact angles were measured on the PV membrane surfaces and the cohesion energy density, together with the solubility parameter of the PVDF membranes, were calculated. The "affinity" of chloroform toward PVDF is higher than that of water; however, the swelling degree of the PVDF membrane is very low because dilute chloroform/water mixtures were used.

A novel theoretical model for VMD process containing no adjustable parameters was developed. The model includes the solution–diffusion flux term through the nonporous portion of the MD membranes as well as a Knudsen flux term, a Poisseuille flux term, and a transition flux term through the membrane pores according to the kinetic theory of gases. From the last three terms of the transport model the effect of the pore size distribution can be studied. Simulation of the VMD performance of water and dilute binary chloroform/water mixture was carried out. It was found that the model could reconstruct the trend observed in the experimental VMD results very well. The pore size and the porosity of the prepared VMD membranes increase with the concentration of water in the PVDF casting solution and the VMD flux increases exponentially with the water content in the PVDF casting solution. The simulation proved fairly accurate in predicting VMD fluxes for pure water but resulted in an overprediction of the permeate concentration for dilute chloroform aqueous mixtures. This may be attributed to the experimental errors because of the high chloroform volatility.

The contribution to the total flux of the solution–diffusion flux through the nonporous portions of the MD membranes decreases as the pore size and porosity increases. For water, it decreases from 30.4% (W0 membrane) to 0.3% (W6 membrane), whereas for chloroform it decreases from 40.1% (W0 membrane) to 0.7% (W6 membrane).

For the MD membranes used in this study, the viscous contribution in the transition region to the total flux may be considered negligible.

When the fluxes were calculated with pore size distributions the results were slightly higher (that is, 0.6–4.1%) than those calculated using only the mean pore sizes.

The temperature polarization effect is higher for the membranes having larger pore size and higher porosity.

The overall polarization coefficient was defined for each compound of the binary mixture, water and chloroform, and higher polarization effect was observed for the organic compound.

The mass transfer coefficient in the liquid phase was determined from the PV experiments with membranes having different thicknesses, and the applicability of the heat and mass transfer empirical correlations, determined for "pure" heat exchangers without mass transfer, was justified.

Acknowledgments

The authors gratefully acknowledge the financial support from the University Complutense of Madrid through its Project PR78/02-10993.

Literature Cited

Bandini, S., A. Saavedra, and G. C. Sarti, "Vacuum Membrane Distillation: Experiments and Modeling," *AIChE J.*, **43**(2), 398 (1997).

Bottino, A., G. Capannelli, S. Munari, and A. Turturro. "Solubility Parameters of Poly(vinylidene fluoride)," *J Polym Sci. Part B: Polym. Phys.*, **26**, 785 (1988).

Gronda, A. M., S. Buechel, and E. L. Cussler, "Mass Transfer in Corrugated Membranes," *J. Membr. Sci.*, **165**, 177 (2000).

Hernández, A., J. I. Calvo, P. Prádanos, and F. Tejerina, "Pore Size Distributions in Microporous Membranes. A Critical Analysis of the Bubble Point Extended Method," *J. Membr. Sci.*, **112**, 1 (1996).

Hickey, P. J., and C. H. Gooding, "Mass Transfer in Spiral Wound Pervaporation Modules," *J. Membr. Sci.*, **92**, 59 (1994).

Huang, R. Y. M., *Pervaporation Membrane Separation Processes*, Membranes Science and Technology Series 1, Elsevier, New York (1991).

Huang, R. Y. M., R. Pal, and G. Y. Moon, "Pervaporation Dehydration of Aqueous Ethanol and Isopropanol Mixtures through Alginate/Chitosan Two Ply Composite Membranes Supported by Poly(vinylidene fluoride) Porous Membrane," *J. Membr. Sci.*, **167**, 275 (2000).

Kesting, R. E., *Synthetic Polymeric Membranes*, 2nd Edition, Wiley, New York (1985).

Khayet, M., C. Y. Feng, K. C. Khulbe, and T. Matsuura, "Preparation and Characterization of Polyvinylidene Fluoride Hollow Fiber Membranes for Ultrafiltration," *Polymer*, **43**, 3879 (2002).

Khayet, M., C. Y. Feng, and T. Matsuura, "Morphological Study of Fluorinated Asymmetric Polyetherimide Ultrafiltration Membranes by Surface Modifying Macromolecules," *J. Membr. Sci.*, **213**, 159 (2003).

Khayet, M., M. P. Godino, and J. I. Mengual, "Nature of Flow on Sweeping Gas Membrane Distillation," *J. Membr. Sci.*, **170**, 243 (2000).

Khayet, M., M. P. Godino, and J. I. Mengual, "Modelling Transport Mechanism Through a Porous Partition," *J. Non-Equilib. Thermodyn.*, **26**, 1 (2001).

Khayet, M., and T. Matsuura, "Preparation and Characterization of Polyvinylidene Fluoride Membranes for Membrane Distillation," *Ind. Eng. Chem. Res.*, **40**, 5710 (2001).

Laganà, F., G. Barbieri, and E. Drioli, "Direct Contact Membrane Distillation: Modelling and Concentration Experiments," *J. Membr. Sci.*, **166**, 1 (2000).

Lawson, K. W., and D. R. Lloyd, "Membrane Distillation: I. Module Design and Performance Evaluation using Vacuum Membrane Distillation," *J. Membr. Sci.*, **120**, 111 (1996).

Lawson, K. W., and D. R. Lloyd, "Review: Membrane Distillation," *J. Membr. Sci.*, **124**, 1 (1997).

Leighton, D. T., and J. M. Calo, "Distribution Coefficients of Chlorinated Hydrocarbons in Dilute Air–Water Systems for Groundwater Contamination Applications," *J. Chem. Eng. Data*, **26**, 382 (1981).

Martínez, L., F. J. Florido-Díaz, A. Hernández, and P. Prádanos, "Characterization of Three Hydrophobic Porous Membranes Used in Membrane Distillation: Modelling and Evaluation of Their Water Vapour Permeabilities," *J. Membr. Sci.*, **203**, 15 (2002).
Mason, E. A., and A. P. Maulinaskas, *Gas Transport in Porous Media: The Dusty Gas Model*, Elsevier, Amsterdam (1983).
Matsuura, T., *Synthetic Membranes and Membrane Separation Processes*, CRC Press, Boca Raton, FL (1993).
Mengual, J. I., M. Khayet, P. Godino, "A Critical Review of the Empirical Heat and Mass Transfer Correlations Used in Membrane Distillation," *Book of Abstracts NAMS 2001*, May 15–20, Lexington, KY, p. 195 (2001).
Mengual, J. I., and L. Peña, "Membrane Distillation," *Colloid Interface Sci.*, **1**, 17 (1997).
Michaels, A. S., L. Nelsen, and M. C. Porter, "Ultrafiltration," *Membrane Process in Industry and Biomedicine*, Bier M., Ed., Plenum Press, New York, p. 197 (1971).
Nakao, S., "Review: Determination of Pore Size and Pore Size Distribution. 3. Filtration Membranes," *J. Membr. Sci.*, **96**, 131 (1994).
Nunes, S. P., and K. V. Peinemann, "Ultrafiltration Membranes from PVDF/PMMA Blends," *J. Membr. Sci.*, **73**, 25 (1992).
Owens, D. K., and R. C. Wendent, "Estimation of the Surface Free Energy of Polymers," *J. Appl. Polym. Sci.*, **13**, 1741 (1969).
Peña, L., J. M. Ortiz de Zárate, and J. I. Mengual, "Steady States in Membrane Distillation: Influence of Membrane Wetting," *J. Chem. Soc. Faraday Trans.*, **89**, 4333 (1993).
Phattaranawik, J., R. Jiraratananon, and A. G. Fane, "Effect of Pore Size Distribution and Air Flux on Mass Transport in Direct Contact Membrane Distillation," *Book of Abstracts ICOM 2002*, July 7–12, Toulouse, France, p. 291 (2002).
Pinnau, I., and B. D. Freeman, *Membrane Formation and Modification*, ACS Symposium Series 744, American Chemical Society, Washington, DC (2000).
Present, R. D., *Kinetic Theory of Gases*, McGraw-Hill, New York (1958).
Schofield, R. W., A. G. Fane, and C. J. D. Fell, "Gas and Vapor Transport through Microporous Membranes. II. Membrane Distillation," *J. Membr. Sci.*, **53**, 173 (1990).
Smolder, K., and A. D. M. Franken, "Terminology for Membrane Distillation," *Desalination*, **72**, 249 (1989).
Urtiaga, A. M., E. D. Gorri, J. K. Beasley, and I. Oritz, "Mass Transfer Analysis of the Pervaporative Separation of Chloroform from Aqueous Solutions in Hollow Fiber Devices," *J. Membr. Sci.*, **156**, 275 (1999).
Urtiaga, A. M., E. D. Gorri, G. Ruiz, and I. Ortiz, "Parallelism and Differences of Pervaporation and Vacuum Membrane Distillation in the Removal of VOCs from Aqueous Streams," *Sep. Purif. Technol.*, **22**, 327 (2001).
Urtiaga, A. M., G. Ruiz, and I. Oritz, "Kinetic Analysis of the Vacuum Membrane Distillation of Chloroform from Aqueous Solutions," *J. Membr. Sci.*, **165**, 99 (2000).
Van Krevelen, D. W., *Properties of Polymers: Their Correlation with Chemical Structure, Their Numerical Estimation and Prediction from Additive Group Contributions*, 3rd Edition, Elsevier, Amsterdam, The Netherlands (1990).
Wilke, C. R., and P. Chang, "Correlation of Diffusion Coefficients in Dilute Solutions," *AIChE J.*, **1**(2), 264 (1955).
Zhang, S., and E. Drioli, "Pervaporation Membranes: Review," *Sep. Sci. Technol.*, **30**(1), 1 (1995).

Manuscript received Apr. 15, 2003, and revision received Nov. 18, 2003.